Applied Acoustics 72 (2011) 226–230

Contents lists available at ScienceDirect

Applied Acoustics

journal homepage: www.elsevier.com/locate/apacoust

Technical Note

Semi-empirical boundary conditions for the linearized acoustic Euler equations using Pseudo-Spectral Time-Domain methods

Carlos Spa [a,*], Jose Escolano [b], Adan Garriga [c]

[a] Departamento de Matemáticas de la Universidad Técnica Federico Santa María (UTFSM), Av. Vicuña Mackenna 3939, Santiago de Chile, Chile
[b] Telecommunication Engineering Department, University of Jaén, E-23700 Linares, Jaén, Spain
[c] International Center for Numerical Methods in Engineering, Azara 4, 07800 Ibiza, Spain

ARTICLE INFO

Article history:
Received 20 April 2010
Received in revised form 27 August 2010
Accepted 3 November 2010
Available online 3 December 2010

Keywords:
Numerical acoustic simulations
Pseudo-Spectral Time-Domain schemes
Impedance boundary conditions

ABSTRACT

Pseudo-Spectral Time-Domain algorithms have emerged as new numerical methods for solving Eulerian problems. These methods, in contrast to more common finite-difference, time-domain approaches, provide isotropic dispersion characteristics. However, the technical literature concerning to this topic presents a serious lack of methods for dealing with partially reflecting boundary conditions in order to simulate surfaces of a specified impedance. In the current paper we present a novel semi-empirical formulation for simulating constant impedance boundary conditions within Pseudo-Spectral techniques based on the Fourier transform. Finally, the validations in one and two dimensions by means of different numerical experiments, show the accuracy of the model.

1. Introduction

The numerical solution of the linearized acoustic Euler equations is a recurrent subject of research in different fields of acoustics such as aeroacoustics [1] and room acoustics [2]. In many acoustic applications, time-domain numerical methods are chosen since they provide accurate solutions in a specific frequency range with an affordable computational cost. Among the different time-domain methods, the Finite-Difference Time-Domain (FDTD) methods are the most used for that purpose [3,4]. However, one of the main drawbacks of FDTD methods is their inherent numerical dispersion which, in most cases, causes misleading results [5]. In the recent years new numerical approaches for solving Eulerian problems have appeared; one of the most interesting approaches is the Pseudo-Spectral Time-Domain (PSTD) methods [6]. In contrast with the common FDTD methods, PSTD methods are characterized by an isotropic dispersion relation [7]. Although they have been successfully applied in many different fields such as acoustic wave propagation [8], piezoelectric transducer modeling [9] or photonic device simulations [10]; the formulation of impedance boundary conditions (BC) is still an open problem [11]. In this paper, a novel algorithm capable of simulating a real-valued frequency-independent impedance BC is presented by using a semi-empirical approach. This novel algorithm provides fairly good results, making it suitable for different applications in acoustics. The paper is organized as follows: in Section 2 we give a brief introduction on the Fourier PSTD method providing a non-staggered algorithm derived from the time-staggered formulation presented by Liu [6]; in Section 3 the proposed algorithm is analyzed in one dimension while in Section 4 we present the two dimensional results for the impedance boundary conditions; finally, in Section 5 the conclusions and forthcoming steps are presented.

2. The PSTD algorithm

In this paper we shall study the linearized Euler equations in one and two dimensions. These equations in two dimensions read [12]:

$$\begin{aligned} &\frac{\partial v_x}{\partial t}+\frac{1}{\rho}\frac{\partial p}{\partial x}=0,\\ &\frac{\partial v_y}{\partial t}+\frac{1}{\rho}\frac{\partial p}{\partial y}=0,\\ &\frac{\partial p}{\partial t}+\rho c^2\left[\frac{\partial v_x}{\partial x}+\frac{\partial v_y}{\partial y}\right]=0, \end{aligned} \tag{1}$$

where ρ is the density of the air and c is the speed of sound. From now on, we shall consider that both ρ and c are constant quantities. The velocity of the air particles is given by $\boldsymbol{v}=(v_x,v_y)$ and p is the acoustic pressure relative to the atmospheric pressure. The first two equations state that a pressure gradient produces an acceleration of the fluid (the air) while the third equation states that a velocity divergence produces a compression of the fluid. These equations are valid for small velocities and small values of the relative pressure.

* Corresponding author.
E-mail address: carlos.spa@usm.cl (C. Spa).

0003-682X/$ - see front matter © 2010 Elsevier Ltd. All rights reserved.
doi:10.1016/j.apacoust.2010.11.002

Although the Fourier spectral PSTD method introduced by Liu [6] was originally formulated for the numerical solution of Maxwell's equations, it can be easily adapted to acoustic wave propagation [8]. This method computes the spatial derivatives in Eq. (1) by using discrete Fourier transforms. In order to illustrate this, let us consider a one dimensional domain of size L and an evolving physical quantity $g(x,t)$. Consider that $\Delta x = L/N_x$ is used as the cell size and N_x is the number of grid points. It is well known that the approximation of the spatial derivative can be written in general as:

$$\frac{\partial g(x,t)}{\partial x} \approx \mathcal{F}_x^{-1}(\imath k_x \mathcal{F}_x(g(x,t))), \tag{2}$$

where $\mathcal{F}_x$ and $\mathcal{F}_x^{-1}$ denote the Fourier transform over the x-axis and its inverse respectively; k_x is the wavenumber and $\imath = \sqrt{-1}$. More concretely, using the discrete Fourier transform, the spatial derivative at the locations $x = i\Delta x$, $i = 0, 1, \ldots, N_x - 1$, is given by a trigonometric polynomial:

$$\left(\frac{\partial g(x,t)}{\partial x}\right)_{x=i\Delta x} = \frac{1}{L}\sum_{m=-N_x/2}^{N_x/2-1} \imath k_m \tilde{g}(m) e^{\imath k_m i\Delta x}, \tag{3}$$

where $k_m = 2\pi m/L$, and $\tilde{g}(m)$ is the Fourier series

$$\tilde{g}(m) = \Delta x \sum_{i=0}^{N_x-1} g(i\Delta x) e^{-\imath k_m i\Delta x}. \tag{4}$$

Interestingly, the discrete Fourier transforms in Eqs. (3) and (4) can be obtained efficiently by using a FFT algorithm [13], with a number of operations of the order of $(N_x \log_2 N_x)$. An explicit form of the PSTD method for the linearized Euler equations in two dimensions (Eq. (1)) can be easily derived,

$$\begin{aligned}
v_x|_{i,j}^{n+1} &= v_x|_{i,j}^{n} - \frac{\Delta t}{\rho}\mathcal{F}_x^{-1}\left(\imath\frac{2\pi n_x}{N_x\Delta x}\mathcal{F}_x(p|_{:,j}^{n})\right),\\
v_y|_{i,j}^{n+1} &= v_y|_{i,j}^{n} - \frac{\Delta t}{\rho}\mathcal{F}_y^{-1}\left(\imath\frac{2\pi n_y}{N_y\Delta y}\mathcal{F}_y(p|_{i,:}^{n})\right),\\
p|_{i,j}^{n+1} &= p|_{i,j}^{n} - \rho c^2\Delta t\mathcal{F}_x^{-1}\left(\imath\frac{2\pi n_x}{N_x\Delta x}\mathcal{F}_x(v_x|_{:,j}^{n+1})\right)\\
&\quad - \rho c^2\Delta t\mathcal{F}_y^{-1}\left(\imath\frac{2\pi n_y}{N_y\Delta y}\mathcal{F}_y(v_y|_{i,:}^{n+1})\right),
\end{aligned} \tag{5}$$

where (i,j) are the two-dimensional spatial coordinates; and Δx and Δy represent the spatial discretization of the two-dimensional lattice. $\mathcal{F}_\mu$ and $\mathcal{F}_\mu^{-1}$ denote the discrete Fourier transform over the μ-axis and its inverse respectively; n_x, and n_y are the index of the Fourier transforms; and the : symbol denotes all μ-coordinate along the straightline cut through the space lattice. Finally, $\imath = \sqrt{-1}$ and N_μ are the total grid points over the μ-axis. The Courant stability condition for the Fourier PSTD method is given by [6]:

$$S = c\frac{\Delta t}{\Delta} \leqslant \frac{2}{\pi\sqrt{D}}, \tag{6}$$

where D represents the dimension (in the case of Eq. (5), $D = 2$). In Eq. (6) we have considered uniform spatial discretization $\Delta = \Delta x = \Delta y$. Note that S in PSTD method is smaller than in FDTD method $(S \leqslant 1/\sqrt{D})$ which means that PSTD is stable for larger cell sizes than FDTD (with the same time discretization step).

A detailed study of the Fourier PSTD scheme, Eq. (5), reveals very interesting properties [6]: firstly, the PSTD method is isotropic, which means that an acoustic pulse propagates at the same speed in all directions (i.e. the dispersion relation is not angle-dependent [5]); secondly, PSTD schemes do not produce phase errors even with two cells per wavelength. These two properties made the PSTD method extremely useful for the acoustic simulation of large domains and when long time solutions are needed. Finally, it is worth noting that the discrete Fourier transforms can be computed very efficiently through the Fast Fourier Transform algorithms [13].

3. One-dimensional boundary conditions

One of the most important parameters in room acoustics is the acoustic impedance, Z, which characterizes the acoustic properties of the materials. This impedance is defined as the ratio between the acoustic pressure and the generated particle velocity normal to the wall [12]. For plane waves striking on a surface with impedance Z, this material property remains constant, independently of the angle of arrival, that means, it reacts locally. Closely related with the acoustic impedance is the reflection factor, R, which is the ratio between incident and reflected pressure waves. In general, the reflection factor is a complex quantity which depends on the frequency and on the direction of the incident wave. Therefore, the acoustical properties of a wall surface are completely described by knowing the reflection factor for each frequency and angle of incidence. From now on we shall restrict our study to real-valued frequency-independent boundary conditions.

In order to implement a partially reflecting BC within the Fourier PSTD method in one dimension, let us consider a one-dimensional domain of length L. The cell size is $\Delta x = L/N_x$, being N_x the number of grid points. The location of the grid points is given by $x = i\Delta x$, with $i = 0, 1, \ldots, N_x - 1$. We propose a semi-empirical boundary equations controlled by a boundary parameter, ξ, which effectively controls the ratio between the acoustic pressure and the velocity, $(p|^{n+1})/(v_x|^{n+1})$. In fact, our proposal for those points that belong to the boundaries, $i = 0$ and $i = N_x - 1$, is:

– ***For*** $\xi \leqslant 1$:

$$\begin{aligned}
v_x|_{i}^{n+1} &= v_x|_{i}^{n} - \frac{\Delta t}{\rho}\mathcal{F}_x^{-1}\left(\imath\frac{2\pi n_x}{N_x\Delta x}\mathcal{F}_x(p|_{:}^{n})\right),\\
p|_{i}^{n+1} &= \xi\left[p|_{i}^{n} - \rho c^2\Delta t\mathcal{F}_x^{-1}\left(\imath\frac{2\pi n_x}{N_x\Delta x}\mathcal{F}_x(v_x|_{:}^{n+1})\right)\right].
\end{aligned}$$

– ***For*** $\xi > 1$:

$$\begin{aligned}
v_x|_{i}^{n+1} &= \frac{1}{\xi}\left[v_x|_{i}^{n} - \frac{\Delta t}{\rho}\mathcal{F}_x^{-1}\left(\imath\frac{2\pi n_x}{N_x\Delta x}\mathcal{F}_x(p|_{:}^{n})\right)\right],\\
p|_{i}^{n+1} &= p|_{i}^{n} - \rho c^2\Delta t\mathcal{F}_x^{-1}\left(\imath\frac{2\pi n_x}{N_x\Delta x}\mathcal{F}_x(v_x|_{:}^{n+1})\right).
\end{aligned} \tag{7}$$

From Eq. (7) it is clear that the new parameter, ξ, has to be related with the impedance of the wall (and hence with the reflection factor) because the impedance is simply given by the ratio of the acoustic pressure and the particle velocity. Therefore, the relation $\frac{p}{v_x}$ at the boundary points has to be proportional to the impedance of the boundary at each time step.

In order to find the relation between the boundary parameter, ξ, and the acoustic impedance, Z, we performed a set of numerical experiments. The experiments were performed on a one dimensional line where an acoustic impulse was located at a relative distance of 50 cells from the wall. The acoustic impulse was approximated by a *sinc* function (a low-pass approximation of Dirac's delta function),

$$p_{\text{source}}^{n} = \frac{\sin(2\pi f(n-n_0)\Delta t)}{2\pi f(n-n_0)\Delta t} \quad n \leqslant 36, \tag{8}$$

which presents a flat frequency spectrum from *0* to *f*. In our experiments we fix the values $f = 2500$ Hz, $n_0 = 19$ and $\Delta t = 1/16{,}000$ s. For each value of ξ we simulate an acoustic impulse, Eq. (8), and we measure the reflection factor for all frequencies from $f = 0$ Hz to $f = 2500$ Hz. The results are shown in Fig. 1 where we plot the parameter ξ as a function of the measured reflection coefficient.

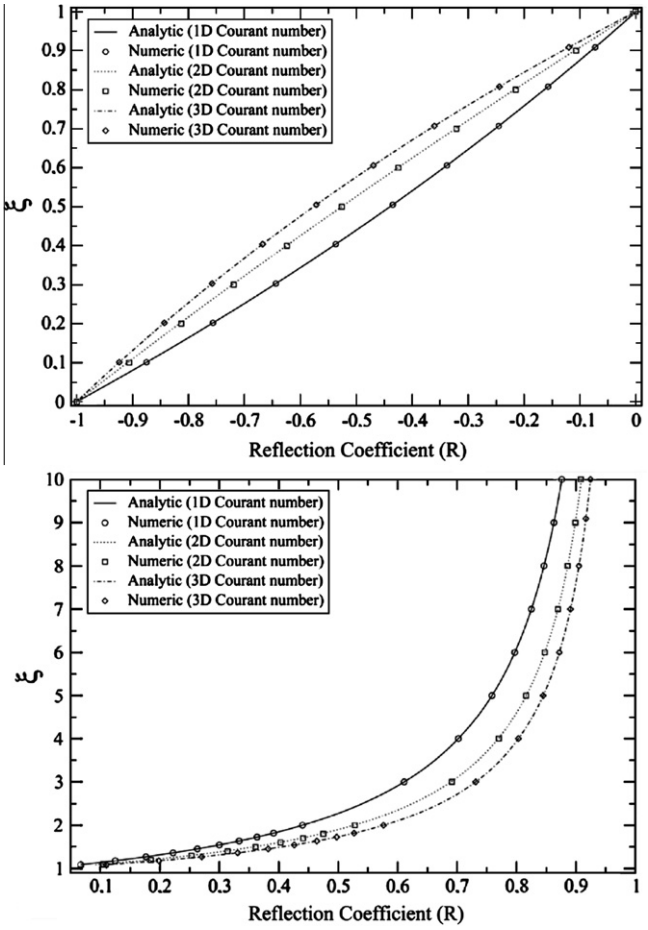

Fig. 1. (Up) Plot of the functional relation between the boundary parameter ξ and the modulus of the reflection coefficient for $\xi \leqslant 1$ in one dimension. The points represent the numerical values obtained for $S = \frac{2}{\pi}, S = \frac{2}{\pi\sqrt{2}}$ and $S = \frac{2}{\pi\sqrt{3}}$, while the lines correspond to Eq. (9). (Down) Plot of the functional relation between the boundary parameter ξ and the modulus of the reflection coefficient for $\xi > 1$ in one dimension. The points represent the numerical values obtained for the same values of S, while the lines correspond to Eq. (10). Error bars are smaller than the symbols.

From the numerical data we can conclude two interesting properties: on the one hand, the numerical reflection coefficients do not depend on the frequency; on the other hand, there is a strong dependence on the Courant stability number, S. More interesting is the fact that from the numerical data we found a simple analytical fit between ξ and R:

– ***For*** $\xi \leqslant 1$:

$$\xi = \frac{1+R}{1+R-2SR}, \tag{9}$$

– ***For*** $\xi > 1$:

$$\xi = \frac{1-R+2SR}{1-R}. \tag{10}$$

In Fig. 1 we can clearly see that the analytic expressions, Eqs. (9) and (10), agree with the numerical data. In these plots we have shown the results for three different values of the Courant stability number, $S = \frac{2}{\pi}, S = \frac{2}{\pi\sqrt{2}}$ and $S = \frac{2}{\pi\sqrt{3}}$ which are the optimum values of S for 1D, 2D and 3D simulations respectively. We have to remark that the analytical expressions, Eqs. (9) and (10) are valid for all values of S tested (data not shown). Obviously, the relation between ξ and R can be rewritten in terms of the acoustic impedance leading to the general expression:

– ***For*** $\xi \leqslant 1$:

$$\xi = \frac{Z/(\rho c)}{S + Z/(\rho c) - ZS/(\rho c)}, \tag{11}$$

– ***For*** $\xi > 1$:

$$\xi = ZS/(\rho c) - S + 1. \tag{12}$$

Finally, we want to mention the fact that we did not found any change in the stability of the PSTD method due to the boundary parameter ξ.

4. Two-dimensional boundary conditions

The results obtained for the one-dimensional case can be easily extended to two dimensions allowing for the construction of a locally reacting impedance BC. As a test system, we consider an infinite acoustic wall parallel to the y-axis where the sound source and the receivers are located in the left hand side (as it is illustrated in Fig. 2).

In order to implement a partially absorbing BC for the acoustic wall of Fig. 2 we follow the same strategy as for the one-dimensional case. Therefore, for those nodes located in the wall, we introduce the boundary parameter ξ in the two dimensional Fourier PSTD equations obtaining the following set of coupled equations:

– ***For*** $\xi \leqslant 1$:

$$\begin{aligned}
v_x|_{i,j}^{n+1} &= v_x|_{i,j}^{n} - \frac{\Delta t}{\rho}\mathcal{F}_x^{-1}\left(\imath\frac{2\pi n_x}{N_x\Delta x}\mathcal{F}_x(p|_{:,j}^{n})\right),\\
v_y|_{i,j}^{n+1} &= v_y|_{i,j}^{n} - \frac{\Delta t}{\rho}\mathcal{F}_y^{-1}\left(\imath\frac{2\pi n_y}{N_y\Delta y}\mathcal{F}_y(p|_{i,:}^{n})\right),\\
p|_{i,j}^{n+1} &= \xi\left[p|_{i,j}^{n} - \rho c^2\Delta t\mathcal{F}_x^{-1}\left(\imath\frac{2\pi n_x}{N_x\Delta x}\mathcal{F}_x(v_x|_{:,j}^{n+1})\right)\right],
\end{aligned}$$

– ***For*** $\xi > 1$:

$$\begin{aligned}
v_x|_{i,j}^{n+1} &= \frac{1}{\xi}\left[v_x|_{i,j}^{n} - \frac{\Delta t}{\rho}\mathcal{F}_x^{-1}\left(\imath\frac{2\pi n_x}{N_x\Delta x}\mathcal{F}_x(p|_{:,j}^{n})\right)\right],\\
v_y|_{i,j}^{n+1} &= v_y|_{i,j}^{n} - \frac{\Delta t}{\rho}\mathcal{F}_y^{-1}\left(\imath\frac{2\pi n_y}{N_y\Delta y}\mathcal{F}_y(p|_{i,:}^{n})\right),\\
p|_{i,j}^{n+1} &= p|_{i,j}^{n} - \rho c^2\Delta t\mathcal{F}_x^{-1}\left(\imath\frac{2\pi n_x}{N_x\Delta x}\mathcal{F}_x(v_x|_{:,j}^{n+1})\right).
\end{aligned} \tag{13}$$

Note that the updating equations for the acoustic pressure in the Eq. (13) only consider the gradient in the x direction, thus taking into account the fact that the wall is parallel to the y-axis.

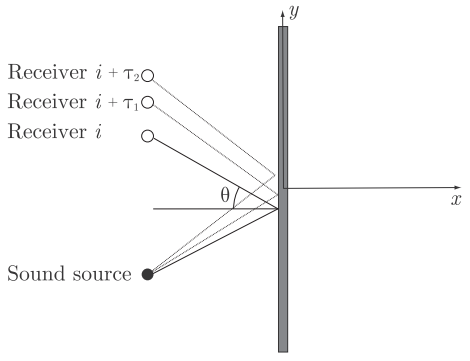

Fig. 2. The two dimensional experimental system. The wall is parallel to the y-axis and both the sound source and the receivers are located in the left hand side. θ is the specular angle defined by the position of the sound source and the receiver.

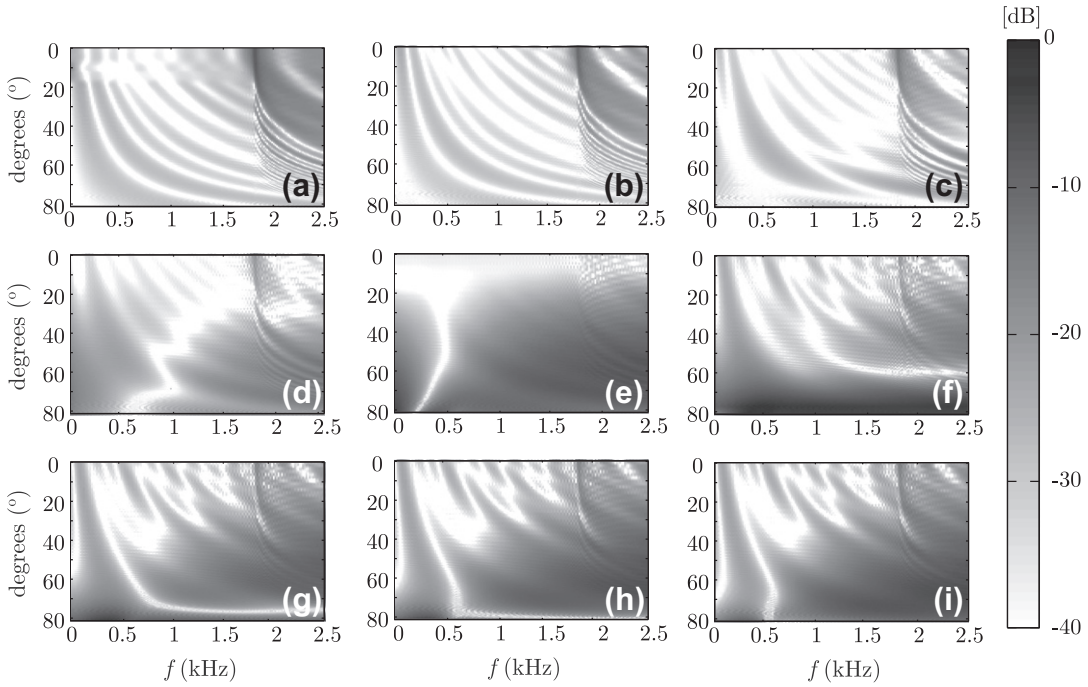

Fig. 3. The error function for different values of ξ as a function of the angle and the frequency. The plots correspond to: (a) $\xi = 0$; (b) $\xi = 0.25$; (c) $\xi = 0.5$; (d) $\xi = 0.75$; (e) $\xi = 1$; (f) $\xi = 2.5$; (g) $\xi = 5$; (h) $\xi = 7.5$; (i) $\xi = 10$.

From Eqs. (11) and (12) we expect that the PSTD scheme in two dimensions produces locally reacting BC according to:

– ***For*** $\xi \leqslant 1$:

$$\xi = \frac{1+R}{1+R+S\cos(\theta)(1-R)-S(1+R)}, \tag{14}$$

– ***For*** $\xi > 1$:

$$\xi = \frac{RS+S+\cos(\theta)(RS-S+1-R)}{\cos(\theta)(1-R)}, \tag{15}$$

where we have considered the two-dimensional relation between the impedance and the reflection coefficient [2], $Z = \frac{\rho c}{\cos(\theta)}\frac{1+R}{1-R}$.

In order to verify the relation between the boundary parameter ξ and the reflection coefficient given by Eqs. (14) and (15), we perform numerical experiments inspired on Ref. [14]. The system consists on a two dimensional rectangular interpolated mesh with a wall placed in the middle of the domain (as it is shown in Fig. 2). On one side of the domain an acoustic impulse is emitted and the resulting responses are computed at the interesting measure points (labeled as receivers in Fig. 2). The goal of this experiment consists on measuring numerically the reflection coefficient, R_{num}, as a function of the angle of incidence (determined by the position of the receivers) and the frequency. A more detailed explanation of this numerical experiment can be found in Ref. [11].

We perform the experiments for different values of the boundary parameter ξ with $S = \frac{2}{\pi\sqrt{2}}$. For each value of ξ, Eqs. (14) and (15) provide an analytic relation between the modulus of the reflection coefficient and the angle of incidence. By comparing the numerical reflection factor, R_{num}, with the theoretical one provided by Eqs. (14) and (15), we can define the following error function:

$$\epsilon = 20\log_{10}\|R - R_{\text{num}}\|, \tag{16}$$

which, as mentioned before, depends in general on the angle of incidence and on the frequency.

The results of the numerical experiments are illustrated in Fig. 3 where we plot the error function, Eq. (16), as a function of the angle of incidence (y-axis) and the frequency (x-axis) for different values of ξ. The error is represented in a graded scale: black corresponds to errors of a few negative dB while color white indicates errors below forty negative dB. The experimental system consisted on a two dimensional domain of 2000×2000 nodes with a wall in the middle (as depicted in Fig. 2). The acoustic impulse generated is just given by Eq. (8) and the receivers were located at places such that the angles of incidence were in the range $\theta \in [0°, 80°]$.

In Fig. 3 we plot the results for nine values of ξ: 0, 0.25, 0.5, 0.75, 1, 2.5, 5, 7.5 and 10 (from (a) to (i) respectively). Thus practically covering the whole range of values of the reflection coefficient. The simulations show remarkable good results for low angles of incidence ($\theta \leqslant 40°$) where the deviations from the analytic relation are lower than -30 dB for all values of ξ. Deviations from the theoretic behavior are more relevant as the angle of incidence increases and for high frequencies. These results can be easily understood taking into account the fact that the number of cells per wavelength for high frequencies is very low; in particular, for $f = 2500$ Hz we have only three cells per wavelength. This value is the result of the time discretization and the Courant number used: $\Delta t = 1/16{,}000$ and $S = \frac{2}{\pi\sqrt{2}}$. This suggests that the results are acceptable for frequencies $f \leqslant 2000$ Hz with the space and time discretizations used in the numerical experiments. Finally, it is worth mentioning the fact that errors below -20 dB correspond to regions in which the modulus of the reflection coefficient itself is very low such as for the case in which $\xi = 1$ (graph *e*) in Fig. 3). Finally we have to stress the fact that we have checked that the numerical data is not distorted by spurious reflections by repeating the simulations with different sizes of the computation domain and by tracking one by one the numerical waves.

5. Conclusions

In the present paper we have introduced a new BC for the Eulerian PSTD methods by introducing in the numerical scheme a boundary parameter, ξ. These BCs have been analyzed numerically both in one and two dimensions. From these studies we have found very useful relations between ξ and the acoustic impedance

(see Eqs. (11) and (12)). The locally reacting behavior of Eqs. (14) and (15) has been tested in two dimensions with proper numerical setup [11,14]. The low errors found indicate that the proposed BCs can be used in many practical acoustic problems within the powerful emerging PSTD techniques.

Therefore, the present study represents a first step towards the implementation of general impedance boundary conditions in PSTD methods. This is a necessary ingredient for many applications in acoustics and for comparing with recent results for FDTD methods in different fields such as room acoustics [15] or outdoor acoustics [16].

It is worth mentioning the fact that, for most practical cases, the presented BCs should be combined with the well-known Perfectly Matched Layer (PML) techniques [17] in order to avoid spurious reflections and the Gibbs effect inherent to all PSTD simulations [18]. Finally, it would be extremely useful to find a theoretical framework to prove the generality of Eqs. (11) and (12).

Acknowledgments

C. Spa has been partially supported by Programa Basal CMM. U. de Chile. A. Garriga is partially supported by the Spanish Ministry of Industry (MITYC) under the project TSI-020100-2008-462 of the Plan Avanza. The work of J. Escolano has been supported by Spanish Ministry of Science and Technology (MCYT) under Project Ref. TEC2009-14414-C03-01 and FEDER funds.

References

[1] Bailly C, Juvé D. Numerical solution of acoustic propagation problems using linearized Euler equations. AIAA J 2000;38(1).
[2] Kuttruff H. Room acoustics. 4th ed. Taylor & Francis; 2000.
[3] Maloney JG, Cummings KE. Adaptation of FDTD techniques to acoustic modeling 11th annual review of progress in applied computational electromagnetics; 1995.
[4] Botteldooren D. Finite-difference time-domain simulation of low-frequency room acoustic problems. J Acoust Soc Am 1995;98:3302–8.
[5] Taflove A, Hagness SC. Computational electrodynamics: the finite-difference time-domain method. Artech House Publishers.
[6] Liu QH. The PSTD algortihms: a time-domain method requiring only two cells per wavelength. Microwave Optical Technol Lett 1997;15:158–65.
[7] Spa C, Mateos T, Garriga A. Methodology for studying the numerical speed of sound in finite differences schemes. Acta Acust United Acust 2009;95(4):690–5.
[8] Liu QH. The pseudospectral time-domain (PSTD) algorithm for acoustic waves in absorptive media. IEEE Trans Ultrason Ferroelectr Freq Control 1998;45(4):1044–55.
[9] Filoux E, Call S, Certon D, Lethiecq M, Levassort F. Modeling of piezoelectric transducers with combined pseudospectral and finite-difference methods. J Acoust Soc Am 2008;123(6):4165–73.
[10] Pernice WHP. Pseudo-spectral time-domain simulation of the transmission and the group delay of photonic devices. Optical Quantum Electron 2008;40:112.
[11] Spa C, Garriga A, Escolano J. Impedance boundary conditions for pseudo-spectral time-domain methods in room acoustics. Appl Acoust 2010;71(5):402–10.
[12] Morse PM, Ingard KU. Theoretical acoustics. Princeton University Press; 1986.
[13] Cooley JW, Tukey JW. An algorithm for the machine calculation of complex Fourier series. Math Comput 1965;19:297–301.
[14] Kelloniemi A, Savioja L, Välimäki V. Spatial filter-based absorbing boundary for the 2-D digital waveguide mesh. IEEE Signal Process Lett 2005;12(2):126–9.
[15] Escolano J, Jacobsen F, López JJ. An efficient realization of frequency dependent boundary conditions in an acoustic finite-difference time-domain model. J Sound Vib 2008;316(1-5):234–47.
[16] Salomons EM, Blumrich R, Heimann D. Eulerian time-domain model for sound propagation over a finite-impedance ground surface. Comparison with frequency-domain models. Acta Acust United Acust 2002;88:483–92.
[17] Bérenger JP. A perfectly matched layer for the absorption of electromagnetic waves. J Comput Phys 1994;114(2):185–200.
[18] Fornberg B. A practical guide to pseudospectral methods. Cambridge, UK: Cambridge University Press; 1996.